First-principles insights into the structure of the incipient magnesium oxide and its instability to decomposition: Oxygen chemisorption to Mg(0001) and thermodynamic stability

M. F. Francis* and C. D. Taylor

Materials Science and Engineering, Los Alamos National Labs, Los Alamos, New Mexico, USA

(Received 22 March 2012; revised manuscript received 19 October 2012; published 28 February 2013)

In this paper, a detailed density functional theory analysis of oxygen binding to Mg(0001) and subsequent clustering is presented. Oxygen monomer adsorption to Mg(0001) is demonstrated to be subsurface. It is shown that magnesium mediates an attractive oxygen-oxygen interaction which ultimately leads to the formation of hexagonal clusters of O* in the tetrahedral-1 site. The structure, work function, and binding properties of oxygen chemisorbed structures are compared with experiment, which allows the unique identification of the tetrahedral-1 site as the low coverage oxygen binding site and the construction of a picture of the early stages of oxide nuclei formation over magnesium. A model of oxide growth at O*/Mg(0001) is proposed. First-principles thermodynamics analysis is used to describe the surface oxide structures and reveals that surface oxides of intermediate oxygen coverage undergo spinodal decomposition. The thermodynamics of an underlying spinodal create an energetic driving force for decomposition of an oxide surface and renewal of a reactive metal interface that may be important in understanding magnesium corrosion. The implications of the findings are that magnesium unalloyed for oxide behavior will always be highly vulnerable to corrosion.

DOI: 10.1103/PhysRevB.87.075450 PACS number(s): 68.43.Bc, 77.84.Bw, 68.35.bd, 82.45.Bb

I. INTRODUCTION

Magnesium and its oxide are of great interest both for their scientific and technical importance. Magnesium is an s-metal or free-electron-like metal making it one of the "simple" metals. MgO is a useful thin film semiconductor as it has a large band gap[1] and is an important catalyst in the petrochemical industry.[2] The metal has a high strength-to-mass ratio,[3] which, were it not for its corrosion problems, would make it useful in lightweight vehicles.[4–6] An oxide passivating layer is often the first line of defense against the corrosion of a structural material, and thus understanding its structure and stability may be central to developing future corrosion resistant magnesium alloys.

When one typically considers the oxide formation of metals, one typically thinks of the more commonly studied late transition metal oxides.[7–16] Reuter and others have performed detailed analysis of oxide nucleation in late transition metals which they have described as a four-step process.[7–19] First, the O_2 dissociates over the metal surface to form chemisorbed oxygen.[20–22] These oxygen atoms remain at the surface where they typically occupy threefold hollow sites.[7] The surface oxygen atoms experience a repulsive O*-O* interaction, which leads to characteristic surface structures.[8–12] Further addition of oxygen only adds to the chemisorbed surface oxygen until, second, a critical surface coverage is exceeded where the oxygen atoms undergo ingress[13] but remain near the surface and do not dissolve into the bulk.[14,15] The critical coverage at which oxygen ingress occurs has been described as the result of a balance between the cost of deforming the lattice to incorporate the oxygen and the repulsive interactions between the adsorbed oxygen adatoms.[13] In the third step of oxide formation over late transition metals, the subsurface oxygen atoms experience mutual attraction and combine to form the first nuclei of oxide formation.[14–16] Continued accommodation of oxygen at the surface ultimately leads to bulk oxide formation, which is the fourth and final stage.[7] A detailed atomic scale understanding of this final step has not yet been achieved.[7] This late transition metal oxide formation process has been referred to as a homogeneous process because the oxide nuclei form out of a homogenously disperse chemisorbed phase.

While magnesium may be referred to as one of the simplest metals, its oxide formation behavior is not consistent with the more familiar late transition metals.[8,23–26] In the first stages of oxide formation over magnesium, O_2 dissociates to form chemisorbed oxygen O*. Rather than adsorbing on the surface, the oxygen atoms are believed to chemisorb in the subsurface.[17,18] These subsurface oxygen atoms attract and form hexagonal clusters which coexist with the clean magnesium surface.[8] Further adsorption of oxygen leads to the formation of a minority square lattice surface structure.[8] The progression from these chemisorbed oxygen clusters to oxide nuclei is not well defined, as these clusters are already subsurface, and the distinction between nuclei and oxide has not yet been made.[23,24]

There are several key features which differ between the more familiar late transition metal oxide nucleation and the free-electron-like magnesium oxide nucleation. Initial dissociative chemisorption of O_2 over magnesium results in subsurface adsorption rather than surface adsorption,[23,24] while in transition metals the result is surface adsorption.[7] Where oxygen ingress is a rate-limiting step in late transition metals,[13–16] it appears to be spontaneous in magnesium.[23,24] Oxygen, apparently repulsive over late transition metals,[8–12] seems to be attractive over magnesium.[8,23,24] Given the absence of a detailed mechanistic description of the initial stages of oxide formation over magnesium and the relevance to numerous technological applications, this paper seeks to perform a first-principles investigation of those energetics that result in the earliest stages of oxide formation in magnesium.

In this paper, first-principles density functional theory (DFT) methods are applied to investigate the structure and energetics which govern oxide nucleation. We look specifically at the forces which ultimately result in the subsurface

adsorption of O* and the attractive magnesium mediated O*-O* interaction. The energetics of probe configurations and their work functions are analyzed in conjunction with data from the literature to help understand oxide nucleation from O_2 at the Mg(0001) surface.

II. METHOD

A. Physical model

The hexagonal close-packed (hcp) structure of magnesium was used with the basal plane as a model surface. In order to simulate a surface-like environment, a six-layer-deep slab with the bottom two layers frozen in a bulklike configuration and the upper-most four layers free to relax was used (see Appendix, Fig. 11); this was done in order to permit surface reconstruction on one side of the slab while simulating a bulklike environment on the other. The simulation method used required a periodic cell. In the periodic cell, a 15-Å gap was created between the upper-most and bottom-most layers in order to simulate a vacuum. A p(6 × 6) model of the Mg(0001) surface was used to reduce image-image lateral interactions. This physical model was chosen in order to accurately capture chemisorption behavior which can be strongly influenced by surface reconstruction and electronic structure.

B. Theory and computation

All calculations were performed using the Vienna *Ab initio* Simulation Package (VASP).[27,28] Calculations were performed using the Perdew–Wang 91 (PW91) generalized gradient approximation (GGA)[29] with a GGA functional applied to construct a self-consistent ultra-soft (US) potential.[30] In calculating the electronic structure of the slab systems, the electrons were not considered to be spin polarized (for selection and computation of the appropriate oxygen reference state, see below). Select configurations were tested with and without spin polarized electrons, but no appreciable difference was found as for the case of the similar free-electron-like O_2/Al(111) study.[31,32] The bulk structure of the hcp magnesium was determined by minimizing the stress tensor, allowing both the cell shape and size to change. The electronic structure of the bulk hcp magnesium was calculated using a Monkhorst–Pack scheme,[33,34] with a 2 × 2 × 1 k-point mesh, equivalent to a 12 × 12 × 1 primitive cell k-mesh. A kinetic energy cutoff of 396 eV was used. In the determination of equilibrium configurations, an energy convergence criterion of 1×10^{-5} eV was used for electronic structure, and an energy convergence criterion of 1×10^{-4} eV was used for ionic relaxations. Work-function calculations were performed by subtracting the Fermi energy from the vacuum energy

$$\varphi = \varepsilon_{\text{vacuum}} - \varepsilon_{\text{fermi}}. \tag{1}$$

Given that an asymmetric, frozen slab model was used to represent the surface, a dipole correction was necessary to correctly determine the Fermi and vacuum energies.[35,36]

For the purposes of this study [O*/Mg(0001) and not O_2], GGA-PW91 was selected as the most practical approach.[37] The oxygen molecule binding energy obtained from density functional calculations will vary according to the details of the exchange correlation functional applied. The local density approximation (LDA) significantly overestimates the binding energy to 7.30 eV (5.23 is the experimental value). The PW91 shares some of these defects of the LDA, overestimating to 6.06 eV, as does the PBE functional (5.99 eV). The revised Perdew-Burke-Ernzerhof functional improves upon this by yielding a value of 5.59 eV. It is clear that improving this description of the molecular double bond is still an emerging story. The recent development of hybrid functionals represents the next step, but the algorithmic heavy lifting required is an obstacle to the full implementation of these functionals for surface chemistry applications. Trends in graphics processing unit computing may alleviate some of these expenses in the near future. Since the PW91 functional provides excellent agreement for the structural properties of Mg metal, and the Mg-O bonding we will explore is chemically distinct from the hard-to-describe O=O bond, we will apply PW91 to understand the surface chemistry that precedes Mg oxidation, restricting ourselves to the use of atomic O as a reference state. Where one seeks to compare binding energies to O_2, one should use the experimental binding energy of 5.23 eV (2.61 eV/O-atom) as the additive constant.

For these reasons, oxygen binding energies to the Mg-surface system are referenced to an oxygen atom in the gas phase (computed using the appropriate spin polarization) and are calculated on a per-atom basis. Two different measures of the binding energy are utilized. Given n oxygen atoms, the average oxygen binding energy per oxygen E_{be} is determined by the following relation between the total energy of the clean magnesium surface E[Mg(0001)], the total energy of an oxygen atom in the gas phase E(O), and the total energy of n oxygen atoms chemisorbed to the Mg(0001) surface $E[n\text{O/Mg}(0001)]$:

$$E_{\text{be}} = \frac{1}{n}(E[n\text{O/Mg}(0001)] - \{E[\text{Mg}(0001)] + nE(\text{O})\}). \tag{2}$$

Also used is the differential binding energy δE_{be}:

$$\delta E_{\text{be}} = E(\text{cluster} + O) - [E(\text{cluster}) + E(O)], \tag{3}$$

in which the differential binding energy is used not to assess the binding of a structure but a new atom bound to a preexisting structure. In Eq. (3), E(cluster) represents the total energy of some oxygen cluster on the Mg(0001) surface, E(cluster + O) is the energy of the cluster with an oxygen atom added, and E(O) is the energy of the O atom in the gas phase. Both the average binding energy E_{be} and the differential binding energy δE_{be} provide different and meaningful information; both of these metrics are provided to the reader in order to gain insights into the most stable structures and the possible stepwise addition of oxygen species. Due to approximations made in the selection of the exchange-correlation functional, no density functional calculation is entirely first principles. For this reason, there remains an inherent, systematic error intrinsic to these calculations, which can be difficult to estimate, due to a partial cancellation of errors and the fact that the exact form of the exchange-correlation functional remains enigmatic. However, previous work by Hammer *et al.*[38] indicates that relative differences in oxygen adsorption energies can be consistently predicted by both LDA and GGA methods to within 0.03 eV. Therefore, we adopt the accuracy threshold of

TABLE I. Bulk parameters calculated in this paper are done so by minimizing the energy with respect to cell size and shape.

Reference	c (Å)	a (Å)	c/a
This work	5.19	3.19	1.63
PW91-GGA	5.18	3.19	1.62
PBE-GGA[a]	5.15	3.18	1.62
Experiment[b]	5.21	3.21	1.62
Experiment[c]	5.21	3.20	1.63

[a]Reference 68.
[b]Reference 69.
[c]Reference 70.

0.03 eV for E_{be} and δE_{be} when comparing oxygen adsorption energies between different sites and clusters in our present model.

III. RESULTS

A. Mg and the clean Mg(0001) surface

Before studying the effects of oxygen chemisorption to the clean Mg(0001) surface, the bulk and surface magnesium properties were calculated and compared with experiment, Table I. Described in Table I are the bulk parameters calculated here, previous calculations from the literature, and some experimentally determined values. The hcp lattice parameter c was here determined to be 5.19 Å, and the lattice parameter a was determined to be 3.19 Å. These calculated lattice parameters were within less than 1% of the experimentally determined lattice parameters. As another measure of structural accuracy, and directly relevant to the study of chemisorption, the interlayer relaxation was calculated and compared with experiment. The interlayer relaxation was calculated as $\Delta_{ij} = (d_{ij} - d)/d$, where the interlayer spacing d_{ij} was taken between the planes i and j with respect to the bulk spacing of $d = 2.605$ Å. The results of the calculations presented here are shown and compared with experiment in Table II. The experimental results for interlayer relaxation have been extrapolated from low energy electron diffraction (LEED) measurements taken at 130, 300, and 400 K with error values $\sim\pm 1\%$.[39] The calculated values are equivalent to the experimental values within the error of the methods used, but importantly capture the unusual outward relaxation of the clean Mg(0001) surface.[39] The outward relaxation of the magnesium has been explained elsewhere and is not discussed here but only presented as it represents a nuance of surface structure that may play an important role in the chemisorption of adatoms.

TABLE II. Relaxation of outermost layers at hcp Mg(0001). Interlayer relaxation here and in reference calculated according to $\Delta_{ij} = (d_{ij} - d)/d$, where the interlayer spacing d_{ij} was taken between the planes i and j with respect to the bulk spacing of $d = 2.605$ Å.

Reference	Δ_{12}(%)	Δ_{23}(%)	Δ_{34}(%)
This work	0.72	<0.01	−0.12
Experiment[a]	1.76	0.0	0.0

[a]Reference 39.

TABLE III. Binding energy of oxygen to surface sites in a p(6 × 6) cell.

Surface site	Binding energy (eV)
Atop	Unstable
Bridge	Unstable
fcc	−7.28
hcp	Unstable
Tet-1	−7.69
Tet-2	−7.62
Oct	−7.16

B. O* chemisorption

After calculating the properties of the clean Mg(0001) surface, the chemisorption properties of O* monomers were determined. Several surface and subsurface sites are available and are represented in the Appendix, Fig. 12. Not shown are the atop and bridge sites, surface sites in which the surface adatom is bound to either one (atop) or two (bridge) surface metal atoms. Calculations showed the atop, bridge, and hcp sites to be unstable for O* monomers (Table III). The calculated data furthermore shows that the most stable monomer O* site is the tetrahedral-1 site. That the hcp site was unstable is unusual and prompted special investigation.

The stability of the hcp site was determined by constructing a one-dimensional potential energy curve (PEC) of the oxygen atom in the plane of the surface. The O* monomer was displaced in small steps, both out of the plane of the surface and into the plane of the surface, not allowing the O* to move, but allowing the surface Mg to optimize and relax about the fixed O*. In so doing, the PEC of O* along the axis formed by the hcp and tetrahedral-1 site was calculated. This PEC describing the stability of the O* monomer is shown in Fig. 1 with the tetrahedral-1 and hcp site positions marked by dashed lines and labeled. The PEC shows a negligible minimum for the hcp site of <0.01 eV.

The preferential stability of the subsurface sites to the surface sites suggested that bulk dissolution of O* might be preferable to subsurface chemisorption. In order to investigate whether bulk dissolution might be favorable, O* monomer binding was probed in the tetrahedral-1 and tetrahedral-2 sites for each interlayer of the model surface, Fig. 2. The calculations demonstrated that O* binds more strongly to the subsurface interstices than the bulklike interstices.

C. Magnesium-mediated attractive O*-O* interaction

Having investigated the binding behavior of O* monomers, the interaction between these monomers was probed. Whether the oxygen-oxygen interaction was attractive or repulsive was determined by comparing the binding energies of nearest neighbors and next nearest neighbors, Fig. 3. The nearest-neighbor configuration was calculated to bind more strongly than the next nearest neighbor, suggesting attractive oxygen-oxygen interactions. In order to further investigate, the binding energy of O*-O* pairs in tetrahedral-1-tetrahedral-1 configurations at lattice separations of one, two, and three lattice parameters as well as tetrahedral-1-tetrahedral-2 configurations

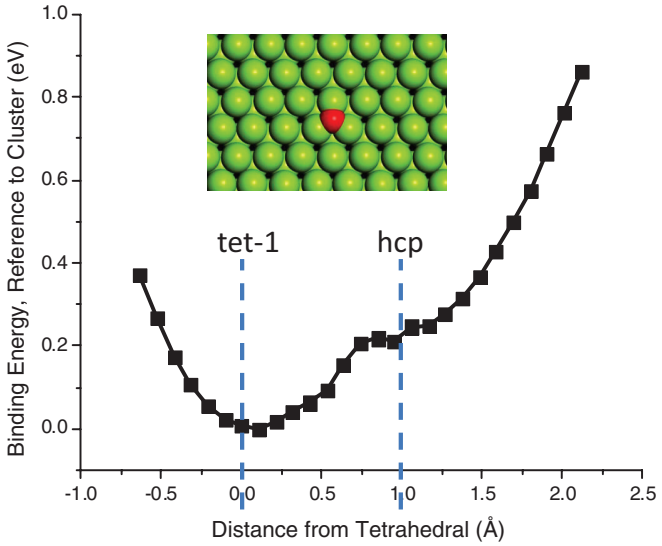

FIG. 1. (Color online) Oxygen binding energy as a function of relative vertical displacement. Binding energy referenced to the energy of a single oxygen atom in the tetrahedral-1 position. The tetrahedral-1 position is defined as zero and the hcp as 1.0 with the position in between scaled appropriately. Positive displacement is out of the surface, negative is into the surface.

at lattice separations of one and one half as well as two and one half lattice parameters was probed, Fig. 4. This sampled the largest O*-O* separation given the p(6 × 6) periodic structure and indicated the O*-O* interaction to be locally attractive. The sampling of interaction versus distance indicates that, for the range of distances that could be studied, the interaction did not become repulsive but rather was locally attractive and then dropped off.

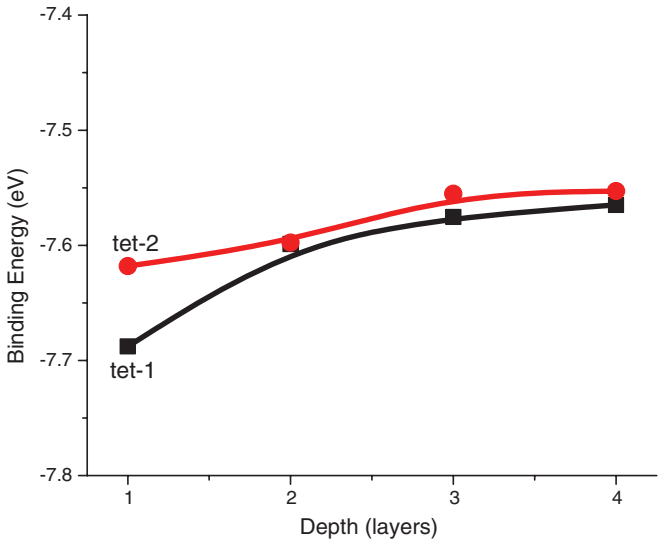

FIG. 2. (Color online) Binding energy of a single oxygen atom to the subsurface tetrahedral-1 (black) and tetrahedral-2 (red) sites as a function of depth. The first layer is defined as the interstices between the magnesium atoms exposed to vacuum and the layer of magnesium atoms immediately below that layer, giving the first layer vacuum-Mg-O-Mg structure.

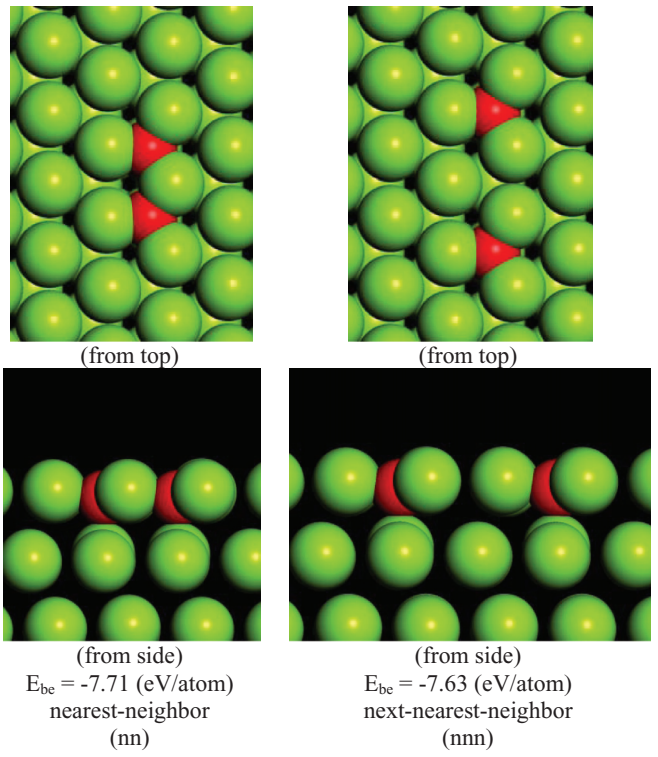

FIG. 3. (Color online) Configurations used for nearest neighbor (left) and next nearest neighbor (right). The images on the top are the view from above the surface, and the images below are a cross-sectional view from the side. Binding energy for configurations calculated on a per-atom basis according to Eq. (2).

D. O* cluster formation

The demonstration of the attractive magnesium-mediated oxygen-oxygen interaction prompted the study of cluster

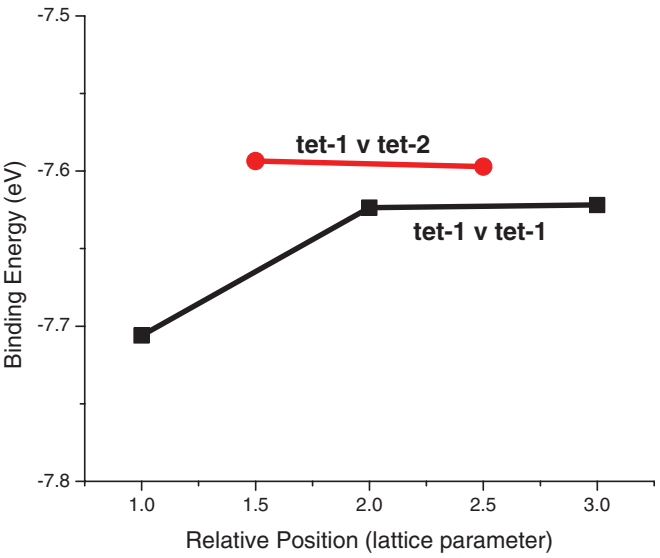

FIG. 4. (Color online) Average binding energy as a function of separation for two oxygen atoms in the tetrahedral-1 and tetrahedral-1 positions (black) and in the tetrahedral-1 and tetrahedral-2 positions (red). The unit of separation is one lattice position on the Mg(0001) surface.

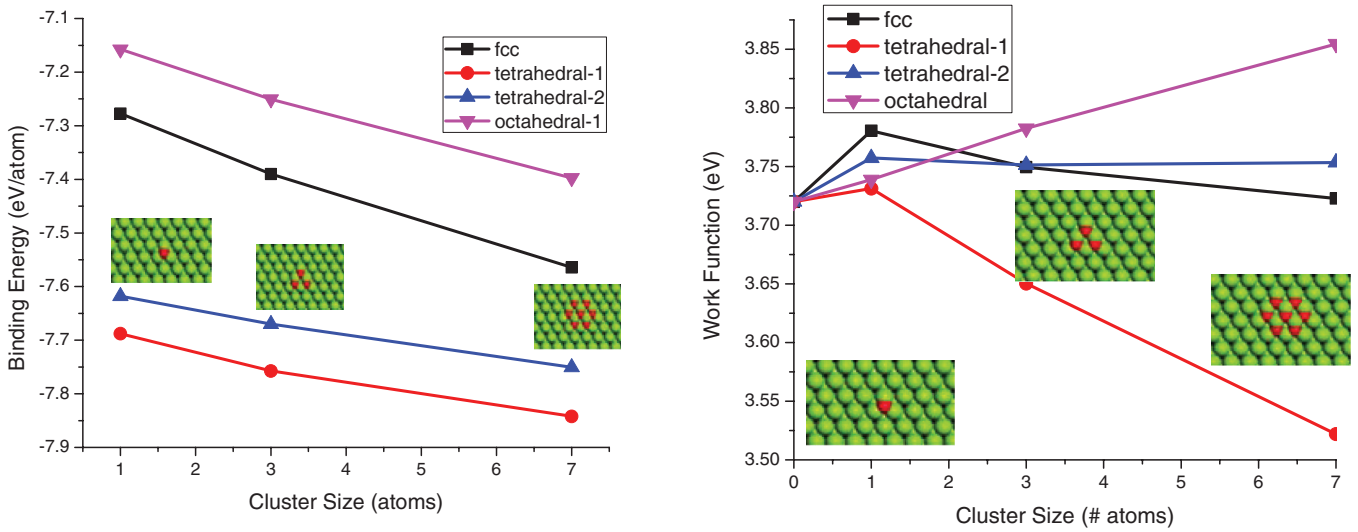

(a) (b)

FIG. 5. (Color online) (a) Binding energy as a function of cluster size for possible oxygen adsorption sites. Each of these calculations used a p(6 × 6) structure. (b) Work function as a function of cluster size for possible oxygen adsorption sites calculated using a p(6 × 6) structure. Clusters as described in text, zero represents a clean surface.

formation. In order to assess the stability of clusters, calculations were performed on clusters as represented in the Appendix, Fig. 13. In the case of each adsorption site studied, larger clusters demonstrated stronger oxygen binding, as will be shown in Fig. 5(a), and furthermore that the subsurface tetrahedral-1 site remained the most stable. Work-function calculations were performed for these clusters, Fig. 5(b). The work function of the clean Mg(0001) surface was calculated to be 3.72 eV. Examining the influence of O* binding to the surface on work function demonstrated that, for the most stable structures, increasing addition of O* reduced the work function further, making it easier to pull electrons out of the surface. Other than the tetrahedral-1 site, chemisorption to all other sites did not reduce the work function. As these tetrahedral-1 O* clusters grow, they nucleate an MgO(111)-like structure. The MgO(111)-like structure has a larger lattice than the underlying Mg(0001) surface and was investigated for induced strain. The surface strain was examined by calculating the surface area of the triangle subtended by the absorbed tetrahedral-1 O* when viewed from above the surface. The area of the triangles was calculated using Heron's formula, and their average area, on a per-O* basis, is shown in Table IV. For each of the examined cluster sizes, the average area of the triangles about the tetrahedral-1 positions was larger than compared to that of the clean Mg(0001) surface. The calculations here were not able to access clusters of larger size, but the attractive O*-O* interaction indicated by binding energy data and the strain indicated by the surface distortion suggests that there may be some intermediate cluster size where the energetic contributions from these factors balance each other out.

TABLE IV. Viewing the surface from the top, the atoms about the tetrahedral-1 site form a triangle. Shown above are the areas of the triangles for the clean surface and tetrahedral-1 clusters. For the three- and seven-atom clusters, an average area is taken. For each area calculation, Heron's formula is used.

Site	Area (Å^2)
Clean	4.5
One-atom tet-1	4.8
Three-atom tet-1	4.8
Seven-atom tet-1	4.7

E. Cluster stabilization of the hcp site

Described in detail, Fig. 1, is the instability of the surface hcp site for an isolated O* monomer. An interesting phenomenon observed in the seven-atom tetrahedral-1 cluster is precisely the opposite of the observed hcp instability—the central atom of the seven-atom cluster is stabilized in an hcp configuration, Fig. 6. The same tests applied to the hcp instability described in Fig. 1 were applied to the central atom of the seven-atom tetrahedral-1 cluster—the central O* atom was pulled in and out of the plane by small increments, kept fixed, and the structure about it allowed to relax. In doing so, a PEC could be constructed and any missed local minima discovered. This stability analysis resulted in the PEC represented in Fig. 6, and we found a stable site only at the surface hcp site for the central O* atom. While the broader meaning of this result is unclear, it does suggest that oxygen agglomeration and subsequent oxide growth over magnesium may proceed in a structurally nontrivial way.

F. Growth from surface clusters

Another strategy taken in this work to gain insights into how cluster growth may occur was to take selected clusters and examine single oxygen atoms binding about those structures. In discussing the possible growth of the oxygen clusters, the differential binding energy, δE_{be} from Eq. (3), was used rather than the average binding energy, E_{be} from Eq. (2). This is not the average energy per oxygen atom, but the change in energy

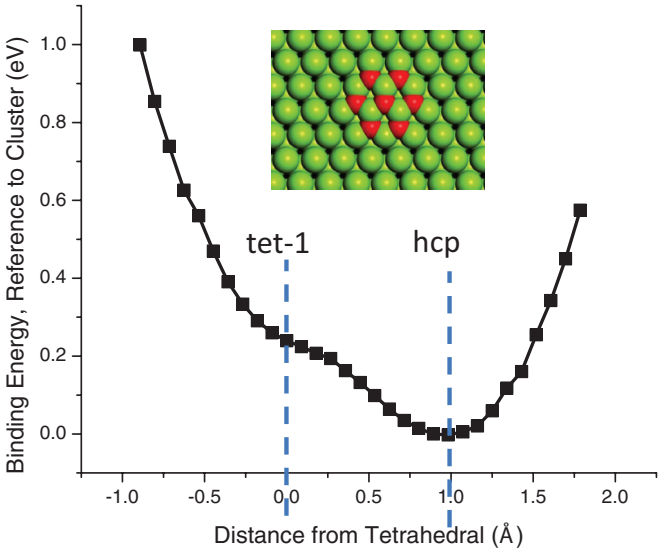

FIG. 6. (Color online) Referenced to the binding energy of a seven-atom tetrahedral-1 O* cluster. Oxygen binding energy as a function of relative vertical displacement, with the tetrahedral-1 position defined as 0.0 and the hcp defined as 1.0. Positive displacement is out of the surface, negative is into the surface.

as the result of adding one oxygen atom. The clusters selected for examination were the three-atom tetrahedral-1 clusters, the seven-atom tetrahedral-1, and an atomic nucleus of MgO(111) embedded in the Mg(0001) surface. The MgO(111) nucleus has the surface structure of the seven-atom tetrahedral-1 with an addition of three oxygen atoms beneath it in the tetrahedral-2 positions. These three-atom, seven-atom, and oxide nucleus structures were selected to address possible two- and three-dimensional growth. Shown in Figs. 7–9 are depictions of these structures with circles representing the selected ad sites. The position of these circles in the images only describe the two-dimensional position of the ad sites. To that end, the circles have been filled in with different colors, where the white circles are ad sites in the first interlayer and on the surface, the grey circles are in the second interlayer, and the black circles are in the third interlayer; in each case, the circles are numbered. The name of the binding sites, the number in the

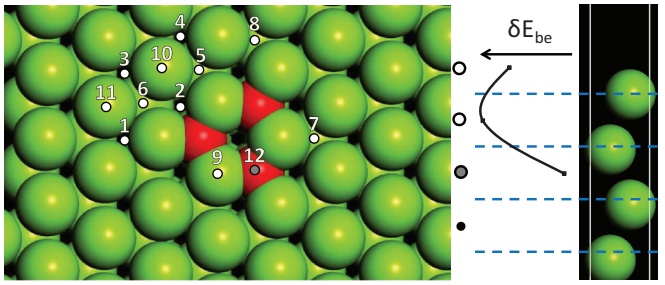

FIG. 7. (Color online) In order to access in which direction the cluster would tend to grow, the binding energy of a single oxygen atom about the three-atom tetrahedral-1 cluster was probed. The position of each probe site is shown in this figure with the binding energies and names in Table V. Each binding site is located consistent with the traditional definition (given in Fig. 12). Sites 1–11 (white circles) are in the first layer, site 12 (gray circle) is in the second layer.

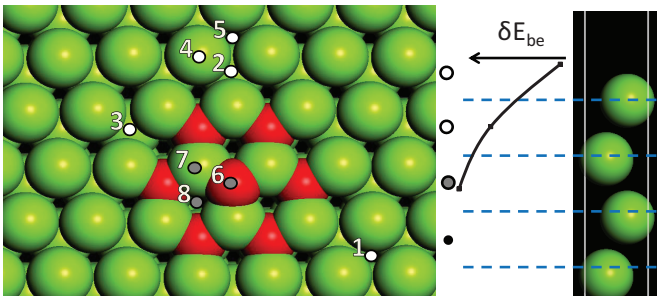

FIG. 8. (Color online) In order to access in which direction the cluster would tend to grow, the binding energy of a single oxygen atom about the seven-atom tetrahedral-1 cluster was probed. The position of each probe site is shown in this figure with the binding energies and names in Table VI. Each binding site is located consistent with the traditional definition (given in Fig. 12). Sites 1–5 (white circles) are in first later, sites 6–8 (gray circles) in the second layer.

figure to which they correspond, and their differential binding energies are listed in the Appendix, Tables V–VII, which correspond to Figs. 7–9, respectively. As a summary tool, insets in Figs. 7–9 are graphical representations of the surface and where the additional oxygen atoms would adsorb. The line in the insets is the strongest bound differential adsorption energy for a certain depth, to the left of which being more strongly bound. The selection of ad sites is not exhaustive but was chosen for intuitive purposes—to understand the driving forces to lateral and vertical growth. The binding energy results suggest that the three-atom clusters would preferably grow laterally, Table V; that the seven-atom cluster would begin to grow subsurface; and that the 10-atom oxide nucleus would begin to add oxygen atoms collinear with the magnesium atoms—intercalating the oxygen atoms in the magnesium plane. It is worth pointing out that these energies are binding energies and not activation energies. They do not

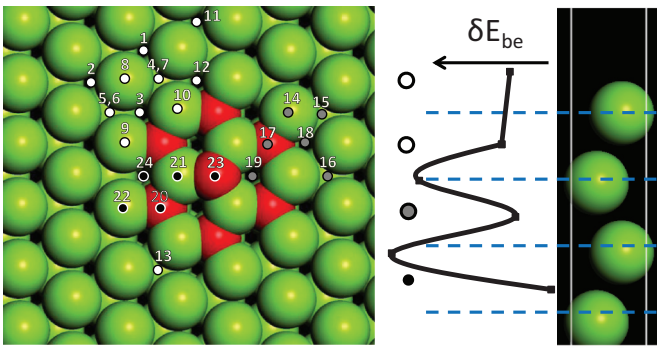

FIG. 9. (Color online) In order to access in which direction the oxide nucleus would tend to grow, the binding energy of a single oxygen atom about a sample MgO(111) nucleus was probed—description of nucleus in text. The position of each probe site is shown in this figure with the binding energies and names in Table VII. Each binding site is located consistent with the traditional definition (given in Fig. 12). Some oxygen deviated from the interstices to be approximately coplanar with the metal atoms—between tetrahedral-1 and tetrahedral-2 sites; those oxygen atoms which deviated in this way are indicated in Table VII. Sites 1–13 (white circles) are in first later, sites 14–19 (gray circles) in the second layer, and sites 20–24 (black circles) are in the third layer.

TABLE V. Binding energy of oxygen atoms in configurations specified in the table and represented by Fig. 7.

	Site	Layer	Differential binding energy (eV)
1	fcc	1	−7.20
2	fcc	1	−7.17
3	fcc	1	−7.10
4	fcc	1	−7.03
5	hcp	1	−7.76
6	hcp	1	−7.55
7	tet-1	1	−7.82
8	tet-1	1	−7.71
9	tet-2	1	−7.92
10	tet-2	1	−7.45
11	tet-2	1	−7.51
12	tet-2	2	−7.43

give any information on the kinetics of oxygen diffusion in the subsurface. In the absence of exhaustive kinetic barrier analysis, no conclusive statement may be made, but the binding energy suggests that, in the thermodynamic limit, the clusters will grow both laterally and vertically.

G. Bader analysis and Redox reactions during island formation

One of the intriguing questions regarding oxidation concerns the transition between the metallic surface state of Mg metal to the formation of an ionic surface film. This transition would be considered from the classical viewpoint in terms of oxidation/reduction chemistry: Atomic O → O^{2-} and atomic/metallic Mg → Mg^{2+}. Although the extraction of such classical concepts from the quantum mechanical description of both molecular and materials systems remains a theoretical holy grail, we have made some attempt to do so using the formalism introduced by Bader. This method, encapsulated in the monograph "Atoms in Molecules: A Quantum Theory", defines charges by integrating between topologically partitioned regions of the electron density that have been identified by some as the boundaries between atoms. A preliminary calculation for the MgO material provides a purely ionic state with +2 and −2 charges for Mg and O, respectively.

For the ultra-dilute case of a singly adsorbed tetrahedral adsorbed O atom (tet-1), the Bader charge on oxygen is calculated to be −2.56. The Bader partitioning identifies a zero-electron region for the second-layer Mg atom immediately below the anion, indicating a cationic Mg^{2+} even at this early stage of the

TABLE VI. Binding energy of oxygen atoms in configurations specified in the table and represented by Fig. 8.

	Site	Layer	Differential binding energy (eV)
1	fcc	1	−6.98
2	hcp	1	−7.73
3	tet-1	1	−7.84
4	tet-2	1	−7.41
5	oct	1	−7.05
6	tet-1	2	−7.63
7	tet-2	2	−7.89
8	oct	2	−7.02

TABLE VII. Binding energy of oxygen atoms in configurations specified in the table and represented by Fig. 9.

	Site	Layer	Differential binding energy (eV)
1	fcc	1	−7.08
2	fcc	1	−7.15
3	fcc	1	−7.24
4	hcp	1	−7.88
5	hcp	1	−7.67
6	tet-1	1	−7.81
7	tet-1	1	−7.91
8	tet-2	1	−7.54
9	tet	1–2 (coplanar)	−7.84
10	tet	1–2 (coplanar)	−8.21
11	oct	1	−7.16
12	oct	1	−7.21
13	oct	1	−7.21
14	tet-1	2	−7.86
15	tet-2	2	−7.61
16	tet-2	2	−7.67
17	tet-2	2	−7.69
18	oct	2	−7.15
19	oct	2	−7.32
20	tet-1	3	−7.73
21	tet-2	3	−7.53
22	tet-2	3	−7.60
23	tet	2–3 (coplanar)	−8.31
24	oct	3	−7.20

oxidation process. The charge on the three surface Mg atoms, which could notionally be considered to be bonded to the O atom, is computed to be −0.52 each. The charge, therefore, is not completely contained within this OMg_4 unit; rather, the charge on this unit amounts to −2.12. The balancing charges are distributed in an approximately oscillating pattern across next and next-next nearest neighbor Mg atoms, both surface and subsurface.

In the seven-atom cluster, the surrounding six tet-1 atoms have a charge of −2.37, whereas the middle pop-up atom has a diminished charge state of −2.07. The three surface atoms that are contained within the seven cluster are, on the other hand, exactly +2 ions. The subsurface Mg atom underneath the central O has an expanded atomic volume and charge, of 7.31 total electrons. This suggests that the volumes of the three surface atoms have condensed with that of the buried Mg atom. The 7.31 electrons spread across four centers are equivalent to 1.83 electrons per atom, or an average charge of +0.17. The subsurface atoms beneath the outer ring of the O_7 cluster all have a cationic +2 state, whereas the perimeter Mg atoms on the surface are neutral. Perimeter subsurface Mg atoms have an anionic state of −1.8, which suggests condensation of the atomic volumes with the subsurface atoms below the outer-ring O sites.

The net picture of this seven-atom oxygen cluster is of anionic O atoms, with charges varying from −2.07 (center atom) and −2.37 for the outer O atoms [$O_7{}^{-16.2}$]. The seven subsurface O atoms and their three nearest neighbors have a distributed charge of [$Mg_{10}{}^{+1.29}$]. Finally, the contribution from the three surface Mg atoms contained within the shape of the cluster, with +2 charge each, is [$Mg_3{}^{+6}$]. Thus, the net

cluster can be represented as $[Mg_{13}O_7]^{-8.9}$. The countercharge is predominantly expressed in partial charging of more distant surface atoms (beyond next-next nearest neighbors). Within the current choice of unit cell, there are six such neighbors, with an average charge of +1.31 electrons each. The remainder of the balancing charge is distributed in peripheral subsurface atoms, but to a lesser extent.

The picture emerging from this Bader analysis, then, is of negatively charged oxide nano-islands (for both the dilute tet-1 type islands, or the larger tet-7 clusters) with strongly polarized Mg and O species similar to the bulk MgO, surrounded by rings of positive charge density.

IV. DISCUSSION

A. Monomer O* chemisorption is tetrahedral-1

The data provided by the calculations here combined with data from the literature help to provide insights into the precise physical structure of the incipient oxide over Mg(0001). The very first stage of oxide formation at the O_2/Mg(0001) interface is the dissociative chemisorption of oxygen.[20–22] O_2 from the gas phase adsorbs as O_2* and undergoes dissociation to form 2O*.[20–22] The binding of oxygen monomers was studied and indicated that the subsurface tetrahedral-1 binds most strongly, Table III and Fig. 1. Furthermore, the oxygen monomers bind preferentially near the surface and will not favorably dissolve into the bulk, Fig. 2. The most commonly reported binding preference of monomer O* on metal surfaces is one of the surface and not subsurface sites.[18] Detailed surface science experiments of oxygen chemisorption to Mg(0001) have been performed.[23,24,40] Both photoelectric and Kelvin work-function measurements show that the work function decreases for initial oxygen chemisorption.[23,24,40] This reduction in work function is contrary to typical electronegative adsorption, which results in an increased work function.[41] Whatever the earliest stages of O* chemisorption is, it must demonstrate a reduction in work function. The calculations here show that the only O* chemisorption which reduces the work function is the tetrahedral-1 site. Comparing theory with experiment points to the most stable O* monomer binding site as tetrahedral-1.

B. Magnesium-mediated O*-O* attraction and subsequent cluster formation

Oxygen-oxygen interactions over the more commonly reported transition metals are found to be repulsive.[18] Here, magnesium-mediated oxygen-oxygen interactions are found to be attractive, Figs. 3 and 4. The demonstration of the attractive magnesium-mediated oxygen-oxygen interaction prompted the study of cluster formation. Investigation into the physical structure of the cluster also found that clustering stabilized the previously unstable surface hcp sites (Fig. 6). In the case of each adsorption site studied, larger clusters demonstrated stronger oxygen binding, Fig. 5(a). Cluster studies furthermore show that tetrahedral-1 clusters uniquely show a reduction in work function, Fig. 5(b).

A host of experimental surface science data provides fertile grounds for comparison to define the precise incipient oxide surface structure.[24] Auger electron spectroscopy (AES) gives a direct sampling of the electronic structure of the entire surface at once. The AES measurements of O_2 exposed to the clean Mg(0001) demonstrate the persistence of peaks associated with a clean Mg(0001) surface from exposures of zero to approximately 3.5 langmuirs, where they become small.[24] Scanning tunneling microscope (STM) experiments have been performed to examine the structural evolution of Mg(0001) with increasing oxygen dosing.[8,25,26,42] The authors found that, at low exposure, the O* readily clustered to form hexagonal structures.[8] Line profiling of the hexagonal structures demonstrated a periodicity of 0.321 nm.[8] X-ray photoelectron diffraction (XPD) measurements, single scattering cluster (SSC) formalism, and DFT studies have been used to study the oxide structure that evolved from Mg(0001).[43–45] This XPD-SSC-DFT study was unable to deduce the precise structure of the low-exposure incipient oxide phase, but they did comment that it had "the same" local geometry as the higher-exposure structures, which were characterized as "flat" and MgO(111)-like[43–45]—the oxygen atoms were approximately in-plane with the magnesium atoms raised from the tetrahedral-1 positions. Work-function experiments of Mg(0001) with increasing oxygen exposure have been performed.[23,24,46] In each of these cases, the work function is found to be reduced by the adsorption of oxygen. Immediately upon exposure to oxygen, the work function begins to reduce linearly with exposure. Around 1.7 to 1.9 langmuirs, the slope of the line changes—the work function remains linear with exposure, but reduces more quickly; see Appendix, Fig. 14(a). The work function continues to reduce with oxygen exposure until 6 ± 1 langmuirs, where it reaches a minimum and then slowly increases once more to values corresponding with MgO. The experimental data taken together indicate cluster formation of a narrow physical structure range and indicate that the clusters reduce the work function.

The tetrahedral-1 subsurface clusters uniquely demonstrate all of the characteristics that are experimentally observed by the incipient oxide. The tetrahedral-1 O* monomers are attractive, driving coexistence of clean and incipient oxide[8,24–26,42] (Figs. 3–5). These clusters have a periodicity identical to the host Mg(0001) lattice of 0.321 nm[8] (Table I), as was observed in STM experiment.[8] The tetrahedral-1 O* clusters uniquely demonstrate a reduction in work function, which corresponds to the observed work function (Fig. 5). Also, while much of the experimental data suggests that first adsorption is subsurface, experiments with 8 L O_2 exposures show that ∼90% of the oxygen atoms are bound to the surface.[47] The calculated "popping" of atoms from the subsurface to the surface (Fig. 6)—that oxygen agglomeration by clusters causes the internal subsurface oxygen atoms to move to the surface—may be an early signature of the later-stage oxide of which there is experimental evidence for oxygen to be on the surface.[47] The experimental and theoretical data combined allow one to assign tetrahedral-1 hexagonal cluster formation to exposures for zero to 1.8 ± 1 langmuirs accompanied by the persistence of clean and O* monomer populated surface.

C. Growth from clusters

At the exposure levels of 1.8 ± 1 langmuirs, the work-function data take on a new slope, suggesting that another

structure, different from the small tetrahedral-1 hexagonal clusters, is nucleating on the surface. The possible growth from small clusters to larger clusters was studied by examining what sites an added oxygen would prefer when added to a three-atom cluster, Table V (Fig. 7), seven-atom cluster, Table VI (Fig. 8), and a nanoscopic oxide nucleus, Table VII (Fig. 9). The cluster growth studies demonstrated that the smallest clusters preferred to grow laterally, then subsurface, and thereafter began to intercalate oxygen in between the magnesium planes (Fig. 9). These nuclei of oxide might serve as the beginning of a later more oxygen-rich structure.

D. The physical structure of the 2-ML and 3-ML magnesium oxide

The multilayer oxide that grows from these clusters has been previously given in detailed combined experimental and theoretical analysis.[43,44] Schröder, Fasel, and Kiejna used x-ray photoelectron diffraction (XPD) measurements, single scattering cluster (SSC) formalism,[45] and DFT to study the oxide structure that evolved from Mg(0001) exposures of 0.15, 1.4, and 8.7 L. Here, DFT was used to find the structure of possible monolayer and multilayer oxide structures;[39,40] SSC was used to simulate the XPD behavior of these DFT determined structures. They found that the multilayered oxide was a mixed 2- and 3-ML structure on top of an almost undistorted Mg(0001) surface and had a graphite-like structure. They referred to this graphite-like structure as "flat" and found that it had a two-dimensional structure in which the oxygen atoms were intercalated in the plane of the magnesium atoms; this is a more complete state of oxide formation of which the beginnings may be inferred from Fig. 9. They furthermore inferred that the rocksalt structure may become more stable at increased exposures and that this "flat" structure was a metastable intermediate. The work provided here and that of Schröder, Fasel, and Kiejna gives a detailed description of the submonolayer and multilayer oxide structure, however, does not give a description of intermediate monolayer oxide structures.

E. Spinodal decomposition at O*/Mg(0001): Phase separation into Mg and oxide

A first-principles thermodynamics (FPT) method based on surface formation energies may be used in conjunction with knowledge of possible stable and unstable structures to gain a deeper understanding into O*/Mg(0001) phase behavior.[48–50] Convex hull phase diagram methods have been successfully used in the solid state community to understand surface phase stability.[51–56] First-principles thermodynamics has had successes, including but not limited to the phase diagram of oxygen adsorbed to Ru, Pd, Pt, and Ag metal surfaces.[51–56] To obtain a precise estimate of the surface formation energy, the free energy of an atom in the bulk phase $F_{\text{bulk}}(T)$ may be compared to the free energy of a surface slab $F_{\text{slab}}(N_{\text{slab}}, T)$. The periodic simulation method requires that a slab of some finite thickness be simulated; the slab will have two surfaces of area A_{slab} exposed to the vacuum and a number of atoms N_{slab}. Periodic simulation methods require that a slab of finite thickness with two sides be simulated with the consequences being that the surface formation energy can be written as

$$\gamma_{\text{clean}}(T) = \frac{F_{\text{slab}}(N_{\text{slab}},T) - N_{\text{slab}} F_{\text{bulk}}(T)}{2A_{\text{slab}}}. \tag{4}$$

Adsorption of oxygen to the surface in some arrangement X from some oxygen source of chemical potential μ_{O} results in a new surface formation energy that can be written as the sum of the clean slab and the changes due to adsorption

$$\gamma_X(T,\mu_{\text{O}}) = \gamma_{\text{clean}}(T) + \Delta\gamma_X(T,\mu_{\text{O}}). \tag{5}$$

The change in surface formation energy for a fixed oxygen coverage Θ_X of some phase X which requires some number of oxygen atoms n_{O} may furthermore be written as

$$\Delta\gamma_X(\Theta_X,\mu_{\text{O}}) = \frac{\Theta_X F_X(T) + (1-\Theta_X)F_{\text{clean}}(T) - [n_{\text{O}}\mu_{\text{O}}\Theta_X + F_{\text{clean}}(T)]}{A}. \tag{6}$$

Writing the change in surface formation energy this way makes explicit that modification of the oxygen chemical potential may change the stable surface state and furthermore that, in considering the stable surface state for a given oxygen coverage, the only factor which is important is the free energy of that state $F_X(T)$. Understanding the stability of surface states for a fixed composition requires only the comparison of the free energies of the surface states allowing one to write

$$\Delta\gamma_{1:2,X}(\Theta_X) = \frac{\Theta_X F_X(T) - [(1-\Theta_X)F_1(T) + \Theta_X F_2(T)]}{A}. \tag{7}$$

Several factors may go into the surface free energy term: Vibrational entropy, zero-point energy, configurational entropy, formation energy, and more.[50] It has, however, previously been demonstrated that the change in entropic contributions between surface states of oxygen over metals is small.[57] There are certainly cases where differences in entropic contributions become important; however, we here approximate the change in formation energy for a given surface coverage as dominated by the change in the 0 Kelvin DFT energy E^{DFT}

$$\Delta\gamma_{1:2,X}(\Theta_X) \approx \frac{\Theta_X E_X^{\text{DFT}}(T) - \left[(1-\Theta_X)E_1^{\text{DFT}}(T) + \Theta_X E_2^{\text{DFT}}(T)\right]}{A}. \tag{8}$$

In this paper and the previous work by Schröder, Fasel, and Kiejna,[43,44] experimental data combined with theoretical analysis has been used to ascribe atomic-scale structure to observation. The structural space sampled between these two datasets may not be considered to be exhaustive, but may be considered to be somewhat representative as they have been

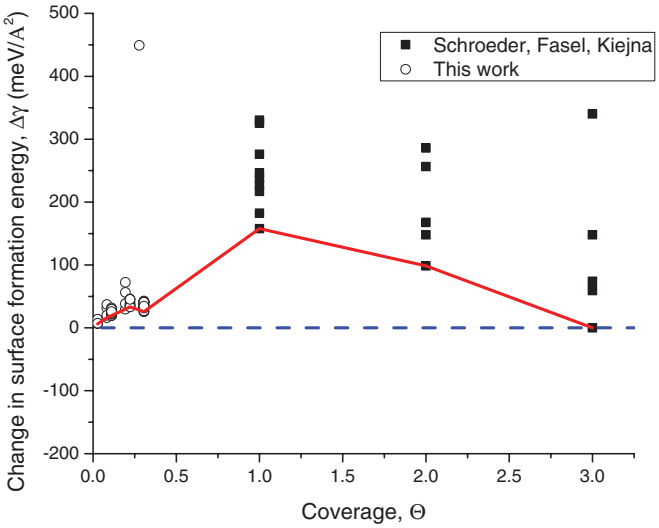

FIG. 10. (Color online) The change in the surface formation energy (Refs. 48–50) as a function of coverage for O*/Mg(0001) structures relative to a clean and 3-ML oxygen structure. Open square data points are taken from this work, and filled triangle data points are taken from work by Schröder, Fasel, and Kiejna (Refs. 39 and 40).

correlated with experimentation. These datasets are used to construct an expression for the relative surface stability of phases with the clean Mg(0001) surface and the most stable calculated 3-ML structure as endpoints

$$\Delta\gamma_X(\Theta) = \left[E^{\mathrm{DFT}}_{X,\Theta}(\Theta) - \left(\Theta E^{\mathrm{DFT}}_{3\mathrm{ML}} - (1-\Theta)E^{\mathrm{DFT}}_{\mathrm{Mg}(0001)}\right)\right]/A_{\mathrm{slab}}. \quad (9)$$

The 3-ML structure is used as an endpoint not because it is believed to be the final state of oxide formation but because it is the thickest of the two sets of data. The choice of the endpoints does not influence the results of the stability analysis—choosing a different endpoint would add or subtract a constant to the free energy at a certain composition and would not change the curvature. The relative stability of the structures presented here and previously[39,40] is presented in Fig. 10 with the solid red line connecting the minimum energy structures and the dotted blue line delineating the tie line.

The strength of the FPT curves is its facility in demonstrating the phase stability of calculated structures. A minimum on an FPT curve would demonstrate a stable phase, but in the particular case of O*/Mg(0001) being studied here, a spinodal decomposition is demonstrated. A spinodal decomposition is driven when an FPT curve demonstrates negative concavity ($\partial^2\Delta\gamma/\partial\Theta^2 < 0$). This results from the fact that anywhere along an FPT curve with negative concavity, the mere diffusive separation of some coverage Θ_o to two separate coverages of slightly enriched $\Theta_o{}^+$ and slightly depleted $\Theta_o{}^-$ would result in a decreased free energy, i.e. self-separation is spontaneous. The inverted U shape of the FPT curve is indicative of underlying negative concavity and the two-phase metal-oxide behavior that may be underlying the reactivity and vulnerability to corrosion of magnesium. If, for example, a 1-ML phase is given and a single atom were to displace from one region to another, two separate regions of 0.9 and 1.1 ML would be created, and the resulting separation would be more stable. Visual analysis of Fig. 10 demonstrates that such a diffusive step is thermodynamically driven and will ultimately lead to phase separation. As a general point, the system will be vulnerable to diffusive separation at a point along the curve that is concave down, which is the case for much of Fig. 10. Experimental evidence of such a phase separation may be found in the O_2/Mg(0001) literature; transmission electron microscope images of Mg(0001) exposed to O_2 demonstrates that platelets of MgO form within the Mg(0001) surface.[58,59] The implications of phase separation of the oxide for corrosion may be important. Phase separation of the oxide means that oxides will tend to be inhomogeneous, that the metal will have prolonged exposure to the environment, and that the reactivity

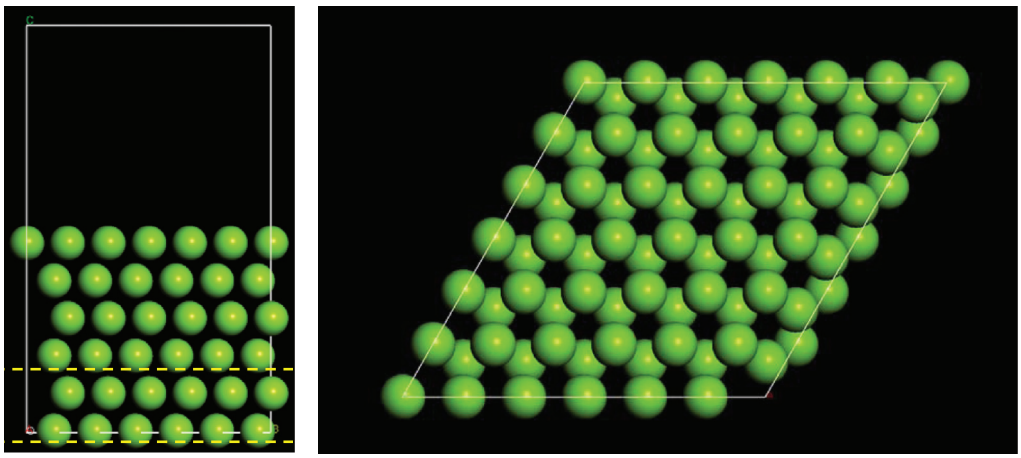

FIG. 11. (Color online) Model surface used in simulations of oxygen chemisorption to Mg(0001)—a p(6 × 6) surface, six atoms deep. Left is the surface viewed from the side, and right is the surface viewed from the top. The yellowed dashed lines in the image on the left are used to highlight the two layers of magnesium that were kept fixed. The four layers of magnesium outside of the dashed lines are those magnesium atoms that were free to relax. Those magnesium atoms interfacing with the vacuum are referred to as the "first" layer, those below as "second", and so on. The space in between the first and second magnesium atoms is referred to as the "first" interlayer, the space between the second and third the "second", and so on.

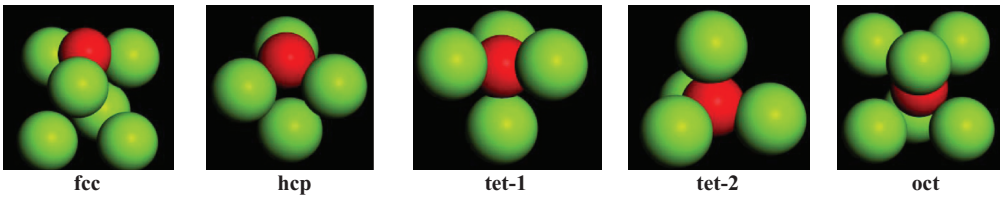

FIG. 12. (Color online) Surface and subsurface sites of oxygen on the Mg hcp(0001) surface—not including atop and bridge. The bold text is the short name for the sites and the longer, roman text is the full name.

of the interface will be greatly increased compared to that of a more homogeneous oxide.

F. A proposed model for oxide growth

The data and analysis presented here allow the creation of a phenomenological model for oxide growth at O_2/Mg(0001). The first stage of oxide growth is the dissociative chemisorption of O_2 to form $2O^*$.[20–22] These O^* monomers chemisorb in the subsurface tetrahedral-1 site. These tetrahedral-1 O^* monomers agglomerate to form clusters. With increasing agglomeration these clusters grow and eventually undergo spinodal decomposition to form clusters of multilayer oxide.[8,25,26,43,44] Subsequent dissociative chemisorption of O_2 results in the preferential growth of the multilayer oxide rather than the renewal of clusters. Those clusters which transformed into multilayer oxide will act as oxide nuclei and agglomeration sites until the oxide growth process is complete.

G. Spinodal decomposition at O*/Al(111)?

Given the more common narrative of homogenous oxide nucleation and the apparently heterogeneous oxide nucleation of magnesium, it is natural to look elsewhere in the literature for another system demonstrating heterogeneous oxide nucleation. It may be that the heterogenous oxide nucleation is driven by spinodal decomposition of which self-separation is an experimental observable. Oxide nucleation at the O_2/Al(111) interface is a very similar heterogeneous process, one in which the oxide self-separates.[31,32,41,60–67] It has been established that, when Al(111) is exposed to O_2, the surface moves from a bare metallic to mixed metallic-chemisorbed oxygen phase to mixed bare metal-chemisorbed oxygen and oxide.[60,64,66] Oxygen clusters or separates to form oxide rather than forming a homogenous chemisorbed oxygen layer. This multiphase self-separated interface at O_2/Al(111) persists until exposures of several hundreds of langmuirs[64,66] and may be indicative of an underlying spinodal decomposition. Verification of a spinodal decomposition at O_2/Al(111) requires direct investigation into first-principles thermodynamics, as presented here. If spinodal decomposition at O_2/Al(111) is verified, the thermodynamic analysis presented here and the many decades of engineering corrosion resistant aluminum alloys may provide a framework for developing more stable magnesium alloys. Given chemical similarities between aluminum and magnesium, borrowing from the decades-long study of aluminum alloys may facilitate the realization of the promise of lightweight magnesium alloys.

V. SUMMARY

In this paper, a detailed density functional theory analysis of the binding of O^* to the Mg(0001) surface was performed and comparison to literature presented in order to construct a detailed picture of the structures that ultimately result in oxide nucleation. The O^* monomers preferably bind to the tetrahedral-1 site and demonstrate stability in the surface face-centered-cubic (fcc) site but not the atop, bridge, or hcp sites. Calculations of oxygen-oxygen-mediated magnesium interactions demonstrated attractive binding which ultimately results in cluster formation. These clusters are of a hexagonal structure with the O^* in the tetrahedral-1 position and have a surface registry equivalent to the underlying Mg(0001) lattice. These clusters are the preferred thermodynamic state to isolated O^* monomers, form at near zero exposures, and have been linked to work-function data. Broader thermodynamic analysis demonstrates that the intermediate oxygen coverages may undergo spinodal decomposition to form local multilayer oxide clusters and clean magnesium. This process of intermediate oxide coverage decomposition may be critical to the corrosion behavior of magnesium as it will drive the system to renew reactive metal interfaces.

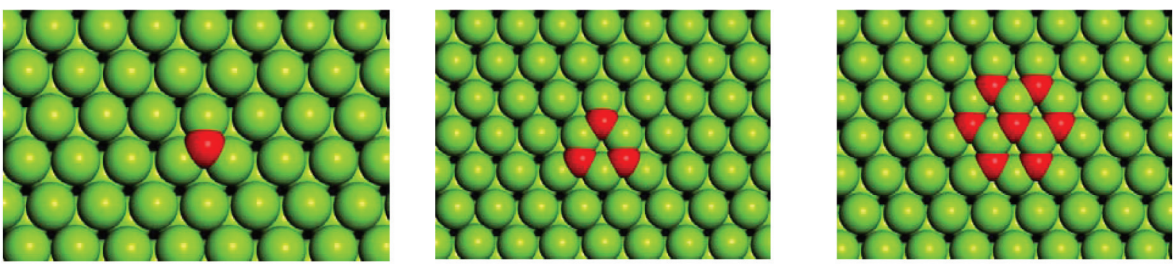

FIG. 13. (Color online) Cluster shapes used for (from left to right) one-, three-, and seven-atom clusters.

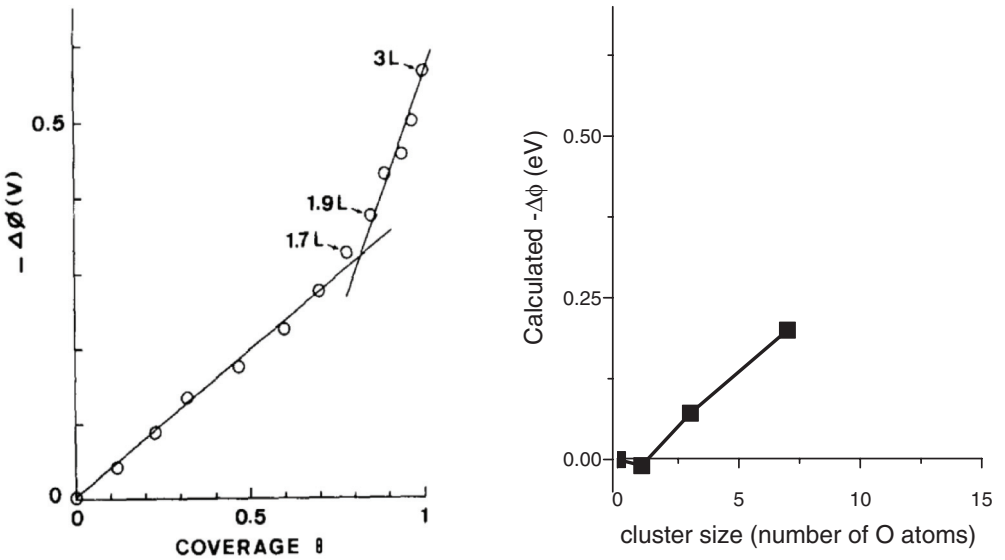

FIG. 14. (a) Work function as a function of exposure for O_2/Mg(0001) as measured by Kelvin probe experiment 24. The coverage is calculated based on a model described in the referenceand the experimental exposures are stated in langmuirs (1 L = 10^{-6} Torr × s). (b) Change in work function for the tetrahedral-1 clusters as a function of cluster size based on calculations presented in Fig. 9(b).

ACKNOWLEDGMENTS

This work was performed at Los Alamos National Laboratory (LANL), using LANL institutional computational resources. The intellectual seeds of this project were developed by the principle author while studying water-aluminum interactions at the University of Virginia. The author is grateful for helpful discussions from Matthew Neurock and Robert Kelly at the University of Virginia as well as Hieu Pham, Edward Holby, Matthew Rossi, and Rafael Leckie at LANL.

APPENDIX

a. Physical model

Figures 11–13 have been given to provide a detailed description of those physical models used in the presented density functional theory calculations.

Represented on the left side of Fig. 11 is the view of the physical model from the side, and in the right-hand side is the view of the physical model from the top. The cell is a p(6 × 6 × 6) hcp(0001) surface. In Fig. 11, a dashed line is given between the second and third most bottom layers. This dashed line is indicated to describe that, below the dashed line, the atoms were fixed in a bulklike configuration; above the dashed line, the atoms were free to relax throughout any and all simulations. The physical model and the constraints were placed in order to give the most realistic representation of surface properties as they are germane to O* chemisorption: Surface electronic structure, bulklike bottom geometry, and large cell size to accommodate strain.

Figure 12 describes those physical adsorption sites germane to this study of O* chemisorption. The full and shorthand name of each configuration is given; green represents Mg, and red represents O; the upper-most green atoms are to be taken as the surface atoms and the others subsurface.

Figure 13 is the top view of the one-, three-, and seven-atom clusters used to directly assess the energies of cluster growth.

b. Work function: Comparison of theory and experiment

Figure 14 is a comparison of experimentally measured work functions and calculated work functions. The left-hand side of Fig. 14 are Kelvin probe measurements of O* chemisorption to Mg(0001); the coverage is based on a model described in the reference, and those labeled exposures on the graph are those that have been experimentally measured. The calculated work function as a function of cluster size is shown in the right-hand side of Fig. 14. The two are presented together as evidence that the clusters are the very first phase of physical chemisorption (not considering monomers) and oxide formation at the O/Mg(0001) interface.

c. Cluster growth: Detailed presentation of data

In the main body of the manuscript, a description of those sites used to assess cluster growth and a graphical representation of the most stable is presented. Tables V–VII present a numerical listing of those data points in those figures for readers interested in a more detailed presentation.

*Present address: Mechanical Engineering, École Polytechnique Fédérale de Lausanne, Lausanne, Vaud, Switzerland.

[1] S. A. Canney, V. A. Sashin, M. J. Ford, and A. S. Kheifets, J. Phys.: Condens. Matter **11**, 7507 (1999).

[2]H. H. U. Heiz and U. Landman, *Nanocatalysis: Principles, Methods, Case Studies* (Springer, Berlin, 2004).
[3]L. Duffy, Materials World **4**, 127 (1996).
[4]H. N. J. Ghijsen, P. A. Thiry, J. J. Pireaux, and P. Caudano, Appl. Surf. Sci. **8**, 397 (1981).
[5]C. R. McGall, M. A. Hill, and R. S. Lillard, Corrosion Eng., Sci. Technol. **40**, 7 (2005).
[6]G. Song and A. Atrens, Advanced Eng. Mater. **5**, 837 (2003).
[7]K. Reuter, arXiv:cond-mat/0409743 (2004).
[8]A. F. Carley, P. R. Davies, K. R. Harikumar, R. V. Jones, and M. W. Roberts, Top. Catal. **24**, 51 (2003).
[9]L. Surnev, G. Rangelov, and G. Bliznakov, Surf. Sci. **159**, 299 (1985).
[10]M. Lindroos, H. Pfnur, G. Held, and D. Menzel, Surf. Sci. **222**, 451 (1989).
[11]H. Pfnur, G. Held, M. Lindroos, and D. Menzel, Surf. Sci. **220**, 43 (1989).
[12]J. M. Hawkins, J. F. Weaver, and A. Asthagiri, Phys. Rev. B **79**, 125434 (2009).
[13]M. Todorova, W. X. Li, M. V. Ganduglia-Pirovano, C. Stampfl, K. Reuter, and M. Scheffler, Phys. Rev. Lett. **89**, 096103 (2002).
[14]K. Reuter, M. V. Ganduglia-Pirovano, C. Stampfl, and M. Scheffler, Phys. Rev. B **65**, 165403 (2002).
[15]L. Wei-Xue, C. Stampfl, and M. Scheffler, Phys. Rev. B **67**, 045408 (2003).
[16]M. V. Ganduglia-Pirovano, K. Reuter, and M. Scheffler, Phys. Rev. B **65**, 245426 (2002).
[17]K. Reuter and M. Scheffler, Phys. Rev. Lett. **90**, 046103 (2003).
[18]K. Reuter and M. Scheffler, Appl. Phys. A **78**, 793 (2004).
[19]M. Todorova, K. Reuter, and M. Scheffler, Phys. Rev. B **71**, 195403 (2005).
[20]J. Behler, B. Delley, S. Lorenz, K. Reuter, and M. Scheffler, Phys. Rev. Lett. **94**, 036104 (2005).
[21]G. Katz, R. Kosloff, and Y. Zeiri, J. Chem. Phys. **120**, 19 (2012).
[22]C. Bungaro, C. Noguera, P. Ballone, and W. Kress, Phys. Rev. Lett. **79**, 4433 (1997).
[23]B. E. Hayden, E. Schweizer, R. Kötz, and A. M. Bradshaw, Surf. Sci. **111**, 26 (1981).
[24]H. Namba, J. Darville, and J. M. Gilles, Surf. Sci. **108**, 446 (1981).
[25]A. F. Carley, P. R. Davies, R. V. Jones, K. R. Harikumar, and M. W. Roberts, Chem. Commun. **2002**, 2020 (2002).
[26]A. U. Goonewardene, J. Karunamuni, R. L. Kurtz, and R. L. Stockbauer, Surf. Sci. **501**, 102 (2002).
[27]G. Kresse and J. Furthmuller, Phys. Rev. B **54**, 11169 (1996).
[28]G. Kresse and J. Furthmuller, Comput. Mater. Sci. **6**, 15 (1996).
[29]J. P. Perdew, J. A. Chevary, S. H. Vosko, K. A. Jackson, M. R. Pederson, D. J. Singh, and C. Fiolhais, Phys. Rev. B **46**, 6671 (1992).
[30]P. E. Blochl, Phys. Rev. B **50**, 17953 (1994).
[31]A. Kiejna and B. I. Lundqvist, Phys. Rev. B **64**, 049901 (2001).
[32]A. Kiejna and B. I. Lundqvist, Phys. Rev. B **63**, 085405 (2001).
[33]H. J. Monkhorst and J. D. Pack, Phys. Rev. B **13**, 5188 (1976).
[34]J. D. Pack and H. J. Monkhorst, Phys. Rev. B **16**, 1748 (1977).
[35]G. Makov and M. C. Payne, Phys. Rev. B **51**, 4014 (1995).
[36]J. Neugebauer and M. Scheffler, Phys. Rev. B **46**, 16067 (1992).
[37]A. Gros, *Theoretical Surf. Sci.: A Microscopic Perspective*, 1st ed. (Springer, Berlin Heidelberg, 2002).
[38]B. Hammer, L. B. Hansen, and J. K. Nørskov, Phys. Rev. B **59**, 7413 (1999).
[39]I. P. Hofmann, A. P. Baddorf, and E. W. Plummer, Phys. Rev. B **66**, 245414 (2002).
[40]T. F. Gesell and E. T. Arakawa, Surf. Sci. **33**, 419 (1972).
[41]R. L. Wells and T. Fort Jr., Surf. Sci. **33**, 172 (1972).
[42]A. F. Carley, P. R. Davies, K. R. Harikumar, R. V. Jones, and M. W. Roberts, Top. Catal. **24**, 9 (2003).
[43]E. Schröder, R. Fasel, and A. Kiejna, Phys. Rev. B **69**, 115431 (2004).
[44]E. Schröder, R. Fasel, and A. Kiejna, Phys. Rev. B **69**, 193405 (2004).
[45]C. S. Fadley, in *Synchrotron Radition Research: Advances in Surf. Sci.*, edited by R. Z. Bachrach (Plenum, New York City, 1990), Vol. 1.
[46]T. F. Gessel and E. T. Arakaw, Surf. Sci. **33**, 3 (1972).
[47]B. C. Mitrovic, D. J. O'Connor, and Y. G. Shen, Surf. Rev. Lett. **5**, 6 (1998).
[48]E. F. Holby, J. Greeley, and D. Morgan, J. Phys. Chem. C **116**, 9942 (2012).
[49]D. D. Lee, J. H. Choy, and J. K. Lee, J. Phase Equilib. **13**, 7 (1992).
[50]R. B. Getman, Y. Xu, and W. F. Schneider, J. Phys. Chem. C **112**, 14 (2008).
[51]Y. Zhang, V. Blum, and K. Reuter, Phys. Rev. B **75**, 235406 (2007).
[52]C. Stampfl, H. J. Kreuzer, S. H. Payne, H. Pfnuer, and M. Scheffler, Phys. Rev. Lett. **83**, 14 (1999).
[53]J. Schnadt, A. Michaelides, J. Knudsen, R. T. Vang, K. Reuter, E. Lægsgaard, M. Scheffler, and F. Besenbacher, Phys. Rev. Lett. **96**, 146101 (2006).
[54]M. Schmid, A. Reicho, A. Stierle, I. Costina, J. Klikovits, P. Kostelnik, O. Dubay, G. Kresse, J. Gustafson, E. Lundgren, J. N. Andersen, H. Dosch, and P. Varga, Phys. Rev. Lett. **96**, 146102 (2006).
[55]H. Tang, A. Van der Ven, and B. L. Trout, Phys. Rev. B **70**, 045420 (2004).
[56]A. Michaelides, K. Reuter, and M. Scheffler, J. Vac. Sci. Technol. A **23**, 1487 (2005).
[57]R. B. Getman and W. F. Schneider, J. Phys. Chem. C **111**, 389 (2007).
[58]R. L. Schwoebel, J. Appl. Phys. **34**, 2776 (1963).
[59]R. L. Schwoebel, J. Appl. Phys. **34**, 2784 (1963).
[60]S. A. Flodstrom, C. W. B. Martinsson, R. Z. Bachrach, S. B. M. Hagstrom, and R. S. Bauer, Phys. Rev. Lett. **40**, 907 (1978).
[61]M. J. Dignam, J. Electrochem. Soc. **109**, 192 (1962).
[62]M. J. Dignam, J. Electrochem. Soc. **109**, 184 (1962).
[63]W. H. Krueger and S. R. Pollack, Surf. Sci. **30**, 263 (1972).
[64]H. Brune, J. Wintterlin, J. Trost, G. Ertl, J. Wiechers, and R. J. Behm, J. Chem. Phys. **99**, 2128 (1993).
[65]T. Wiederholt, H. Brune, J. Wintterlin, R. J. Behm, and G. Ertl, Surf. Sci. **324**, 91 (1995).
[66]J. Trost, H. Brune, J. Wintterlin, R. J. Behm, and G. Ertl, J. Chem. Phys. **108**, 1740 (1998).
[67]A. Kiejna, Phys. Rev. B **68**, 235405 (2003).
[68]J. Zhang, D. W. Zhou, L. P. He, P. Peng, and J. S. Liu, J. Phys. Chem. Solids **70**, 32 (2009).
[69]G. V. Raynor and W. Hume-Rothery, J. Inst. Met. **65**, 379 (1939).
[70]P. Villars and L. D. Calvert, *Pearson's Handbook of Crystallographic Data for Intermetallic Phases*, Vol. 1–3 (American Society for Metals, Ohio, 1986), p. 3258.